Proceedings of IMECE 2003
2003 ASME International Mechanical Engineering Congress and R&D Expo
November 15-21, 2003, Washington, D.C. USA

IMECE2003-41251

3–DIMENSIONAL HYBRID CONTINUUM–ATOMISTIC SIMULATIONS FOR MULTISCALE HYDRODYNAMICS *

Wijesinghe, H.S.
Massachusetts Institute of Technology,
Cambridge, MA
Email: sanith@mit.edu

Hornung, R.
Lawrence Livermore National Laboratory,
Livermore, CA
Email: hornung@llnl.gov

Garcia, A.L.
San Jose State University,
San Jose, CA
Email: algarcia@algarcia.org

Hadjiconstantinou, N.G.
Massachusetts Institute of Technology,
Cambridge, MA
Email: ngh@mit.edu

ABSTRACT

We present an adaptive mesh and algorithmic refinement (AMAR) scheme for modeling multi–scale hydrodynamics. The AMAR approach extends standard conservative adaptive mesh refinement (AMR) algorithms by providing a robust flux–based method for coupling an atomistic fluid representation to a continuum model. The atomistic model is applied locally in regions where the continuum description is invalid or inaccurate, such as near strong flow gradients and at fluid interfaces, or when the continuum grid is refined to the molecular scale.

The need for such "hybrid" methods arises from the fact that hydrodynamics modeled by continuum representations are often under–resolved or inaccurate while solutions generated using molecular resolution globally are not feasible. In the implementation described herein, Direct Simulation Monte Carlo (DSMC) provides an atomistic description of the flow and the compressible two–fluid Euler equations serve as our continuum–scale model. The AMR methodology provides local grid refinement while the algorithm refinement feature allows the transition to DSMC where needed. The continuum and atomistic representations are coupled by matching fluxes at the continuum–atomistic interfaces and by proper averaging and interpolation of data between scales.

Our AMAR application code is implemented in C++ and is built upon the SAMRAI (Structured Adaptive Mesh Refinement Application Infrastructure) framework developed at Lawrence Livermore National Laboratory. SAMRAI provides the parallel adaptive gridding algorithm and enables the coupling between the continuum and atomistic methods.

NOMENCLATURE

A signed area of a grid cell face
c mass concentration of reference fluid species
D diffusion coefficient
d atomic diameter
e total energy density
δF refluxing correction
$\mathbf{F}$ flux vector
k Boltzmann's constant
M reduced mass
m atomic mass
N number of particles per cubic mean free path
n number density

*THIS WORK WAS PERFORMED UNDER THE AUSPICES OF THE U.S. DEPARTMENT OF ENERGY BY UNIVERSITY OF CALIFORNIA LAWRENCE LIVERMORE NATIONAL LABORATORY UNDER CONTRACT NUMBER W-7405-ENG-48.

$\hat{n}$ surface normal
P pressure
$\mathbf{p} = (p_x, p_y, p_z)$ vector of momentum densities
$\mathbf{r}$ particle position vector
S surface element
T temperature
Δt time step
t time
$\mathbf{U}$ Euler solution state vector
$\mathbf{u} = (u_x, u_y, u_z)$ fluid velocity vector
$\mathbf{v}$ particle velocity vector
$\Delta x, \Delta y, \Delta z$ grid spacing

Greek
λ particle mean free path
Ω fluid volume element
$\partial\Omega$ boundary of fluid element
ρ mass density
σ standard deviation

Subscripts/Superscripts
0 mean
1,2 first, second species
α particle index
c continuum
i,j,k coordinate indices
max maximum
p particle
n temporal index
x,y,z spatial coordinates

INTRODUCTION AND BACKGROUND

Multi–scale simulation of complex physical systems has received increasing attention in recent years. The primary challenge lies in resolving physical phenomena occurring over a broad range of spatial and temporal scales. Often, this challenge cannot be met by conventional, single-method formulations. Efficient multiscale formulations respond to this challenge by limiting the use of an expensive high–resolution model (e.g., atomistic) to the regions in which it is needed, while using a simpler, less expensive method, in the rest of the computational domain. Such a hybrid approach allows effective use of the each method in different regions of the problem (e.g., interior and exterior of a shock wave).

Numerous hybrid methods have been proposed and demonstrated for solids [1, 32, 36], liquids [14, 19, 29, 30], and gases [2, 3, 11, 16, 26, 28, 31, 37, 39]. The method described here is the first to combine the full capabilities of adaptive mesh refinement with algorithm refinement.

In what follows, we will first describe the continuum and atomistic methods and their coupling. Next, the challenging question of choosing reliable grid and algorithm refinement criteria to track fluid interfaces is discussed. Finally, we present numerical results from several test cases and compare them with theory and other simulations to verify our approach.

ADAPTIVE MESH AND ALGORITHMIC REFINEMENT

This section describes the Adaptive Mesh and Algorithm Refinement (AMAR) methodology in which a continuum algorithm is replaced by a particle algorithm at the finest grid scale in a hierarchical adaptive grid refinement (AMR) setting. Details of the general AMAR scheme have been presented elsewhere [16]. We will summarize them here for completeness and note differences from previous work.

AMR Algorithm for Continuum Hydrodynamics

In the AMAR implementation described herein, we employ a structured AMR grid hierarchy on which we solve the compressible, two-species Euler equations on every grid level except the finest. On the finest level, the solution is represented by the Direct Simulation Monte Carlo (DSMC) method. Note that AMAR uses the same adaptive meshing and time integration algorithms developed for continuum modeling of shock hydrodynamics [7, 8].

Consider the Euler equations in conservative integral form

$$\frac{d}{dt}\int_{\Omega} \mathbf{U} dV + \oint_{\partial\Omega} \mathbf{F}\cdot\hat{n} dS = 0 \qquad (1)$$

where,

$$\mathbf{U} = \begin{pmatrix} \rho \\ p_x \\ p_y \\ p_z \\ e \\ \rho c \end{pmatrix} \quad ; \quad \mathbf{F^x} = \begin{pmatrix} \rho u_x \\ \rho u_x^2 + P \\ \rho u_x u_y \\ \rho u_x u_z \\ (e+P)u_x \\ \rho c u_x \end{pmatrix} \qquad (2)$$

Here, we provide only the x-direction component of the flux terms; other directions are similar. We assume a two-species gas with the mass concentrations of the two species being c and $(1-c)$; generalization to more species is straight-forward. Discrete time integration is achieved by using a finite volume approximation to Equation 1. This yields a conservative finite difference expression with $\mathbf{U}^n_{ijk}$ appearing as a cell-centered quantity at each time level and $\mathbf{F}^{x,n+\frac{1}{2}}_{i+\frac{1}{2},j,k}$ located at faces between cells at half-time levels. We use a second-order version of an unsplit Godunov scheme to approximate the fluxes [12, 13, 33].

Time stepping on an AMR grid hierarchy involves interleaving time steps on individual levels [8]. Each level has its own spatial grid resolution and timestep (typically constrained by a CFL condition). The key to achieving a conservative AMR algorithm is to define a discretization for Equation 1 that holds on every region of the grid hierarchy. In particular, the discrete cell volume integrals of **U** and the discrete cell face integrals of **F** must match on the locally-refined AMR grid. Thus, integration of a level involves two steps: solution advance and solution synchronization with other levels. Synchronizing the solution across levels assumes that fine grid values are more accurate than coarse grid values. So, coarse values of **U** are replaced by suitable cell volume averages of finer **U** data where levels overlap, and discrete fine flux integrals replace coarse fluxes at coarse-fine grid boundaries. Although the solution is computed differently in overlapping cells on different levels as each level is advanced initially, the synchronization procedure enforces conservation over the entire AMR grid hierarchy.

Atomistic Algorithm

Due to our interest in gas flows [20–23], the atomistic algorithm we use is the direct simulation Monte Carlo (DSMC) method [10]. In DSMC, the state of the system is given by positions and velocities of particles, $\{\mathbf{r}_\alpha, \mathbf{v}_\alpha\}$. The system evolves in time using the following two step approach. First, particles are moved without interaction; that is, their positions are updated to $\mathbf{r}_\alpha + \mathbf{v}_\alpha \Delta t_\mathrm{p}$, where Δt_p is a DSMC timestep. Appropriate boundary conditions are applied to particles that reach the boundary of the DSMC domain. Second, after all particles have moved, a given number are randomly selected for collisions. Rather than exactly calculate successive collisions, as in molecular dynamics [5], the DSMC method generates collisions stochastically with scattering rates and post-collision velocity distributions determined from the kinetic theory of a dilute gas. Accuracy of the splitting of streaming and collisions requires the time step Δt_p to be a fraction of the mean collision time τ_m for a particle [17, 18]. DSMC has been rigorously shown to provide accurate solutions to the Boltzmann equation in the limit as the number of particles becomes large and the DSMC collision cell size and time step become small [40].

Although DSMC is orders of magnitude faster than molecular dynamics for simulation of gases, it is orders of magnitude slower than continuum algorithms for solving partial differential equations of hydrodynamics. Thus, only flow regions that require molecular resolution are treated by DSMC in the AMAR approach.

Continuum–Atomistic Coupling

During time integration of continuum grid levels, fluxes computed at each cell face are used to advance the solution **U** (Figure 1(b)). Continuum values are advanced using a time increment Δt_c appropriate for each level, including those that overlay the DSMC region. When the particle level is integrated, it is advanced to the new time on the finest continuum level using a sequence of particle time steps, Δt_p. The relative magnitude of Δt_p to the finest continuum grid Δt_c depends on the finest continuum grid spacing Δx (typically a few λ) and the particle mean collision time.

Euler solution information is passed to the particles via buffer cells surrounding the DSMC region. At the beginning of each DSMC integration step, particles are created in the buffer cells using the continuum hydrodynamic values (ρ, **u**, T) and their gradients (Figure 1(c)). Since the continuum solution is advanced first, these values are time interpolated between continuum time steps for the sequence of DSMC time steps needed to reach the new continuum solution time. DSMC buffer cells are one mean free path wide; thus, the time step Δt_p is constrained so that it is extremely improbable that a particle will travel further than one mean free path in a single time step. The particle velocities are drawn from an appropriate distribution for the continuum solver, such as the Chapman–Enskog distribution [15].

During each DSMC time integration step, all particles are moved, including those in the buffer regions (Figure 1(d)). A particle that crosses the interface between continuum and DSMC regions will eventually contribute to the flux at the corresponding continuum cell face during the synchronization of the DSMC level with the finest continuum level. After moving particles, those residing in buffer regions are discarded. Then, collisions among the remaining particles are evaluated and new particle velocities are computed.

After the DSMC region has advanced over an entire continuum grid timestep, the continuum and DSMC solutions are synchronized in a manner analogous to the AMR level synchronization process described earlier. First, the continuum values in each cell overlaying the DSMC region interior are set to the conservative averages of data from the particles within the continuum grid cell region (Figure 1(e)). Second, the continuum solution in cells adjacent to the DSMC region is recomputed using a "refluxing" process (Figure 1(f)). That is, a flux correction is computed using a space and time integral of particle flux data,

$$\delta F = -A\mathbf{F}^{n+\frac{1}{2}} + \sum_{\text{particles}} F_p. \tag{3}$$

The sum represents the flux of the conserved quantities carried by particles passing through the continuum cell face during the DSMC updates. Finally,

$$\mathbf{U}^{n+1} = \overline{\mathbf{U}^{n+1}} + \frac{\Delta t_\mathrm{c} \delta F}{\Delta x \Delta y \Delta z} \tag{4}$$

is used to update the conserved quantities on the continuum grid

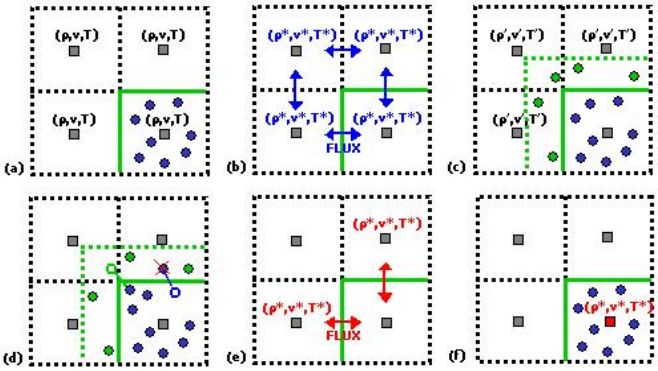

Figure 1. Outline of AMAR hybrid: (a) Beginning of a time step; (b) Advance the continuum grid; (c) Create buffer particles; (d) Advance DSMC particles; (e) Refluxing; (f) Reset overlying continuum grid.

where $\overline{\mathbf{U}^{n+1}}$ is the coarse grid solution before computing the flux correction.

In summary, the coupling between the continuum and DSMC methods is performed in three operations. First, continuum solution values are interpolated to create particles in DSMC buffer cells before each DSMC step. Second, conserved quantities in each continuum cell overlaying the DSMC region are replaced by averages over particles in the same region. Third, fluxes recorded when particles cross the DSMC interface are used to correct the continuum solution in cells adjacent to the DSMC region. This coupling procedure makes the DSMC region appear as any other level in the AMR grid hierarchy.

Multiple DSMC parallelepiped regions (i.e., *patches*) are coupled by copying particles from patch interiors to buffer regions of adjacent DSMC patches. That is, particles in the interior of one patch supply boundary values (by acting as a reservoir) for adjacent particle patches. After copying particles into buffer regions, each DSMC patch may be integrated *independently*, in the same fashion that different patches in a conventional AMR problems are treated after exchanging boundary data.

Refinement Criteria

Criteria for refining the mesh and transitioning from continuum to a particle scheme is a significant research topic and is generally problem specific. Standard AMR methods assume that the differential equations are valid at all length scales in the computation and grid refinement is often based on ad hoc notions (e.g., refine around steep gradients) or analytical error estimation techniques involving the continuum differential equations (e.g., Richardson extrapolation). In contrast, hybrid methods apply computational models matched to the flow properties at each physical scale. While results presented later demonstrate that we can effectively focus DSMC locally to capture shocks and diffusion fronts, many research issues remain.

The AMAR algorithm can refine the grid and algorithm based on any of a number of possible criteria. However, we have found that for single species flows, refinement based on density gradients is reliable. Tracking concentration gradients or concentration values within some interval are effective for multi–species flows involving concentration interfaces. Parameters for transitioning to DSMC are based on the continuum breakdown parameter method proposed by Bird [9], i.e., refinement is triggered by spatial gradients exceeding continuum tolerances. The gradient detector formula that we use is a variation of a sharp discontinuity detector by Trangenstein and Pember [38].

Due to spontaneous stochastic fluctuations in DSMC computations, it is important to track gradients in a manner that does not allow the fluctuations to trigger unnecessary refinement and excessively large DSMC regions. Let us consider the gas density as an example. Using the fact that for an ideal gas under equilibrium conditions the number of particles in a given volume is Poisson distributed, it can be shown that the standard deviation in the normalized density gradient is [24],

$$\sqrt{\left\langle \left(\frac{d\rho/dx}{\rho} \right)^2 \right\rangle} \approx \sqrt{\left\langle \left(\frac{N_{i+1} - N_i}{\Delta x \langle N_i \rangle} \right)^2 \right\rangle} = \frac{\sqrt{2}}{\Delta x \sqrt{\langle N \rangle}} \qquad (5)$$

where N is the number of particles in a cell where macroscopic properties are defined. The fluid density fluctuation can only be reduced by increasing the number of DSMC simulation particles. This has consequences for the use of density gradient tolerances R_ρ used for AMAR. In general, such tolerances must be based on the number of particles used for the atomistic domain since the spatial gradients of density on the *coarse* grid which is fluctuating (as shown below) are used to decide whether refinement will take place. In particular, in our version of density-gradient-based refinement, refinement occurs in regions where the non–dimensionalized density gradients are above the R_ρ threshold, i.e.

$$R_\rho < \frac{2\lambda}{\rho} \left| \frac{d\rho}{dx} \right| \qquad (6)$$

Note that the density gradient is calculated in the continuum mesh on a coarser AMR hierarchy level than the DSMC level.

To determine the minimum value of R_ρ required to prevent growth of the atomistic region, simulations were conducted using the domain geometry shown in Figure 2 for a range of N. Grid refinement occurs during a "trigger" event where the density fluctuations exceed R_ρ and the atomistic subdomain grows in the axial direction by a single continuum cell width. The value of R_ρ that yields a $5-10\%$ trigger rate (i.e. between 5-10 trigger events per 100 iterations) is plotted in Figure 3 as a function of N. In what follows we outline how theoretical predictions bounding

these numerical results, shown as solid lines in Figure 3, can be obtained.

For the geometry considered in this test problem, each continuum cell consists of 8 DSMC cells and hence effectively the contribution of $8 \times N$ particles is averaged to determine the density gradient between continuum cells. From Equation (5) for continuum cells,

$$\sigma = \sqrt{\left\langle \left(\frac{d\rho/dx}{\rho} \right)^2 \right\rangle_c} \approx \frac{1}{2\Delta x \sqrt{\langle N \rangle}} \qquad (7)$$

Note that we are assuming that the fluctuation of the continuum cells across from the atomistic–continuum interface is approximately the same as that in the atomistic region. This was shown to be the case for the diffusion equation and a random walk model in [4], and is verified here for the Euler–DSMC system as shown in Figure 4. This allows the use of Equation (5) that was derived assuming 2 atomistic cells. Note that the observed trigger event is a composite of a large number of probable density gradient fluctuations that could exceed R_ρ; gradients across all possible nearest neighbor cells, next-to-nearest neighbor cells and diagonally-nearest neighbor cells are all individually evaluated by the refinement routines and checked against R_ρ. For a 10% trigger rate (or equivalent probability of trigger) the probability of an individual cell having a density fluctuation exceeding R_ρ can be estimated as $O(0.1/100)$ by observing that,

1. since the trigger event is rare, probabilities can be taken as additive,
2. for the geometry considered, there are ≈ 300 nearest neighbor, next–nearest neighbor and diagonal cells that can trigger refinement and
3. the rapid decay of the Gaussian distribution ensures the decreasing probability ($O(0.1/100) \sim O(0.001)$) of a single event does not significantly alter the corresponding confidence interval and thus an exact enumeration of all possible trigger pairs with correct weighting factors is not necessary.

For example our probability estimate at $O(0.001)$ suggests that our confidence interval is $3\sigma - 4\sigma$. This is verified in Figure 3. Larger trigger rates can be achieved by reducing R_ρ. Curves shown in Figure 3 help prototype tolerance criteria using a small number of particles prior to running larger simulations.

CODE AND ALGORITHM VERIFICATION TESTS

This section describes a number of test problems used to verify the AMAR hybrid formulation. Tolerance parameters used for grid refinement are also described. The single–species tests use gaseous Argon (molecular mass $m = 6.63 \times 10^{-23}$ g, hard sphere diameter $d = 3.66 \times 10^{-8}$ cm) at atmospheric conditions ($P = 1.013 \times 10^5$ Pa and average temperature $\overline{T} = 273$ K). This choice is for convenience reasons. The hard sphere diameter for Argon is well–known to reproduce equilibrium and non–equilibrium properties accurately. Argon is also used in a large number of DSMC studies and thus a substantial literature base of simulation and experimental results exist for verification purposes.

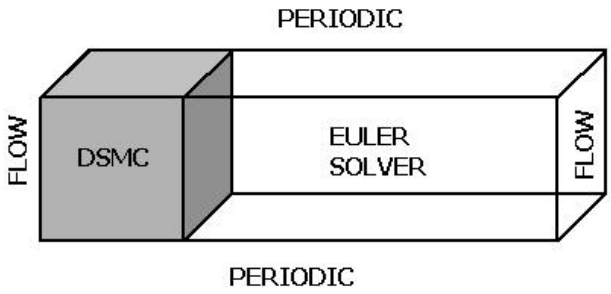

Figure 2. 3D AMAR computational domain for investigation of tolerance parameter variation with number of particles in DSMC cells.

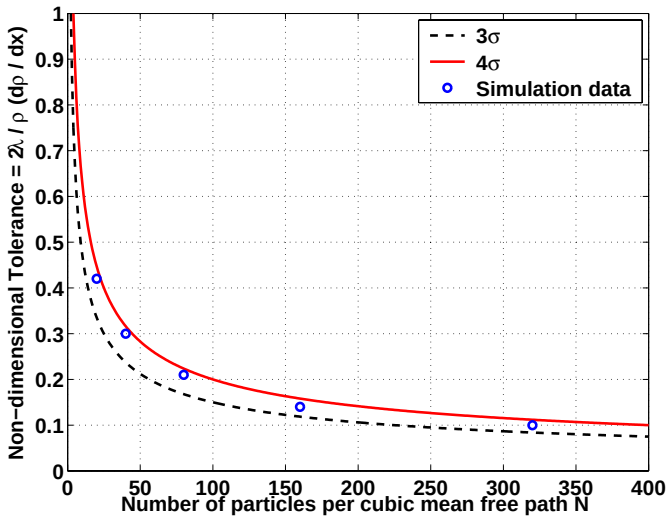

Figure 3. Variation of density gradient tolerance with number of DSMC particles N.

Thermodynamic Equilibrium

We performed a number of uniform field tests to investigate the conservation properties of the hybrid scheme and to understand the effect of particle fluctuations on the continuum subdomain. A domain which consists of a cubic DSMC region of size $4\lambda \times 4\lambda \times 4\lambda$ embedded in the center of an Euler continuum grid of size $32\lambda \times 32\lambda \times 32\lambda$ was utilized. The DSMC computation uses 800 particles per λ^3. The continuum cell size is 2λ, while the DSMC grid size is λ. Periodic boundary conditions are ap-

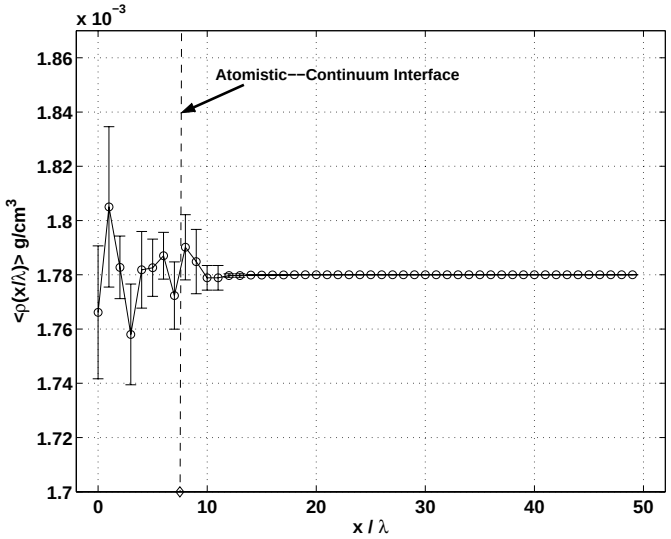

Figure 4. Average density for stationary fluid Euler–DSMC hybrid simulation with $N_c = 80$. Errorbars give one standard deviation over 10 samples.

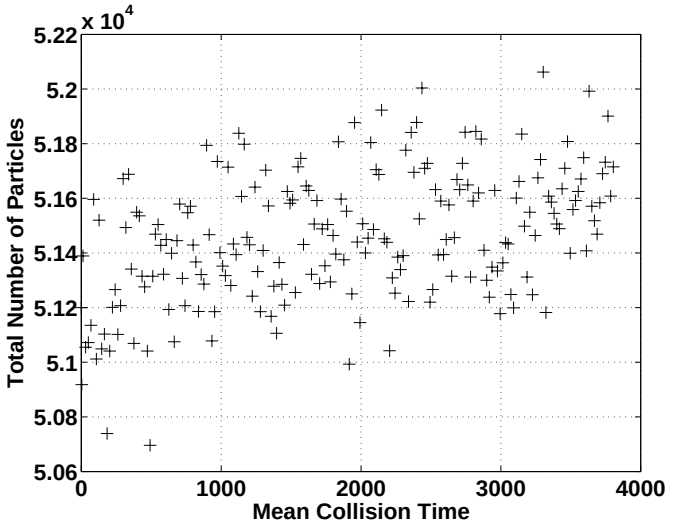

Figure 5. Particle increase in the DSMC domain resulting from net heat flux transfer from the DSMC to the Euler region.

plied at each face of the cubic domain. This geometry is the same as in [16] for comparison purposes. The density and temperature field were initialized at $\rho = 1.78 \times 10^{-3} g/cm^3$ and $T = 273K$ and the initial velocity field was set to zero in all directions.

Although the initial conditions are uniform, the statistical nature of atomistic solution generates fluctuations that transfer heat flux to the continuum subdomain. Since the Euler model possesses no mechanism to transfer thermal energy back to the atomistic domain, the result is an energy increase in the continuum subdomain and a corresponding energy decrease in the atomistic subdomain as total energy is conserved. This, in turn, produces an increase in density in the atomistic subdomain so as to maintain mechanical equilibrium (i.e., constant pressure). This is evident by the increase in the total number of particles in the atomistic subdomain as shown in Figure 5. This phenomenon has been observed in other Euler/DSMC hybrid schemes [16]. We have additionally found the particle increase in the atomistic subdomain to be reduced in the presence of an imposed uniform flow field. This is currently under investigation.

Concentration Diffusion

Concentration diffusion tests were conducted to verify the ability of AMAR to track the spreading of an interface between two gases. The Euler model contains no diffusion terms (except for artificial numerical dissipation) so spreading of the interface is governed by physics modeled by the DSMC routines.

The diffusion coefficient for two gases modeled as hard spheres can be approximated as [25],

$$D_{12} = \frac{3}{16} \frac{\sqrt{2\pi k^3 T^3 / M}}{P \pi d^2} = \frac{3}{8} \frac{1}{nd^2} \sqrt{\frac{kT}{2\pi M}} \qquad (8)$$

where $M = (1/m_1 + 1/m_2)^{-1} = m_1 m_2/(m_1 + m_2)$ is the reduced mass, and $d = (d_1 + d_2)/2$ is the average atomic diameter.

A simple concentration diffusion test involves Argon gas either side of an interface "colored" differently, i.e., the gases are essentially isotopes with negligible mass differences that undergo self–diffusion. The self–diffusion coefficient for Argon at standard temperature and pressure is $D_{11} = 0.14\ cm^2/s$. Figure 6 shows the evolution of the atomistic–continuum computational domain for this self–diffusion test. Initially the red (left) and blue (right) gases are separated by a discontinuous interface corresponding to a step function profile for the gas concentration. The gradient of the corresponding mass concentration is used to place the atomistic region at the gas interface at the initial time. Subsequently, the mixing region is tracked using a "mass–concentration–value" refinement criteria which triggers below 0.001 and above 0.999. These values ensure negligible concentration gradients exists across atomistic–continuum interface.

The hybrid concentration profiles for the self–diffusion case are compared with theoretical profiles in Figure 7. Also shown is the concentration profile for a test case using Argon and a fictitious gas G with hard–sphere diameter $d_2 = 1.516 \times 10^{-8}$cm such that the diffusion coefficient is twice the self–diffusion coefficient; that is, $D_{12} = 2 \times D_{11} = 0.28\ cm^2/s$. The simulation results show excellent agreement with theory in both cases.

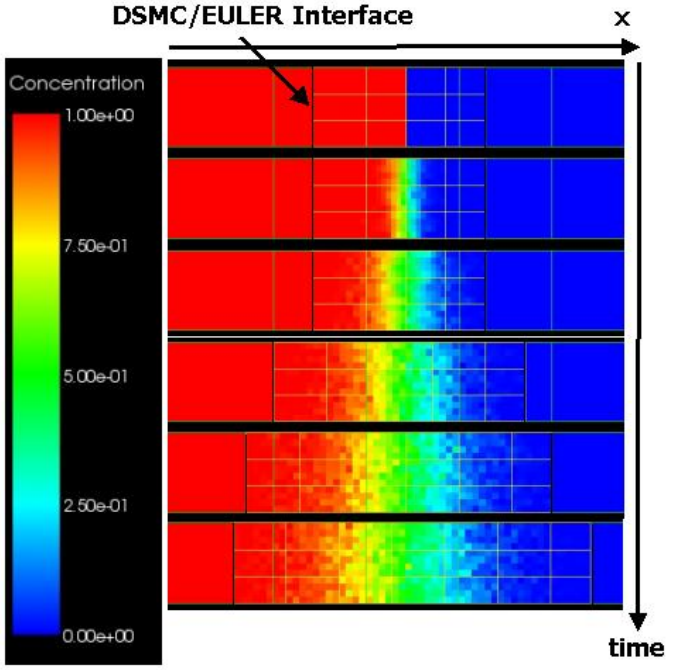

Figure 6. Computational domain for self-diffusion interface tracked adaptively. The borders of DSMC patches are indicated by the boxes near the middle of the domain. The Euler model is applied elsewhere.

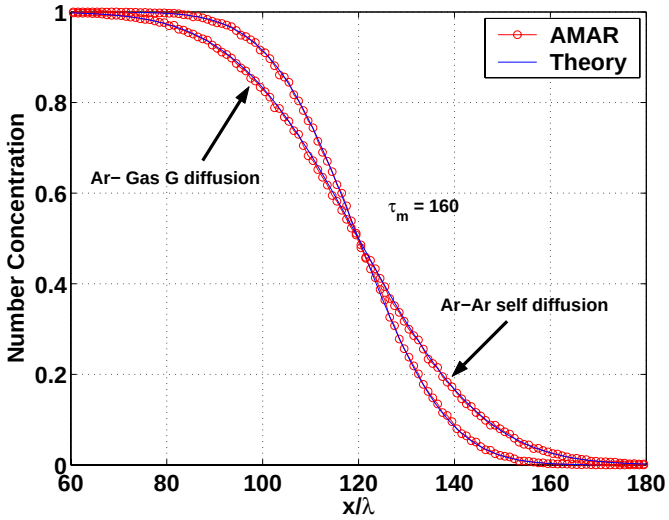

Figure 7. Comparison of profiles obtained simulating diffusion with AMAR with theoretical diffusion profiles. Both self-diffusion and two-species diffusion are shown. Note λ refers to the Ar-Ar mean free path. The mean collision time τ_m is also associated with the Ar-Ar system.

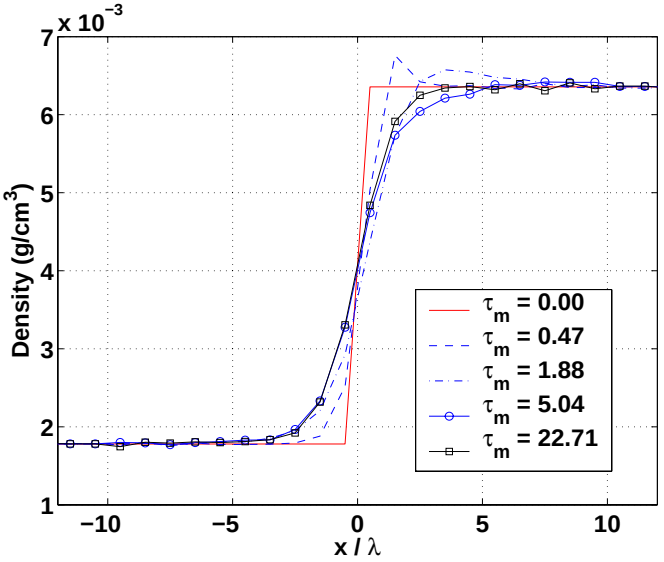

Figure 8. Argon gas density profile relaxation to equilibrium. τ_m is the mean collision time.

Stationary Shock Waves

Stationary shock simulations were conducted for both a single gas and a binary gas mixture.

Single Gas Stationary Shock Wave For the single gas case, a shock wave is initialized using the discontinuous step profile given by the Rankine–Hugoniot conditions for Argon gas with an upstream Mach number of 5.0. The shock wave density, temperature and velocity ratios for this Mach number are 3.57, 8.68 and 0.28, respectively. A density gradient tolerance parameter $R_\rho = 0.2$ was used to detect and refine the continuum grid across the shock. This value for R_ρ creates a stable $\pm 10\lambda$ atomistic region ahead of and behind the shock front.

The time evolution of the density profile is shown in Figure 8. The initial step profile gradually transitions to a smoother curved profile within 20 mean collision times. The final equilibrium profiles for the pressure, density, velocity and temperature are shown in Figure 9. The hybrid solution matches the analytical solution in the far field while resolving the flow discontinuity at the shock front. Note since the initial density gradient in the streamwise direction is essentially infinite, the shock region will be refined for any setting of R_ρ. As the profile becomes smoother however, the value of R_ρ is critical to ensure the shock front remains tagged for refinement while preventing excessive atomistic subdomain growth due to spurious statistical fluctuations. This is achieved successfully with the $R_\rho = 0.2$ setting.

Binary Gas Stationary Shock Wave The binary gas shock simulation was conducted using a mixture of Helium and Xenon gases with number densities of 97% and 3% respectively. The hard sphere mass and diameter chosen to model Helium and Xenon were $m_1 = 6.65 \times 10^{-24}$g, $m_2 = 2.18 \times 10^{-22}$g and

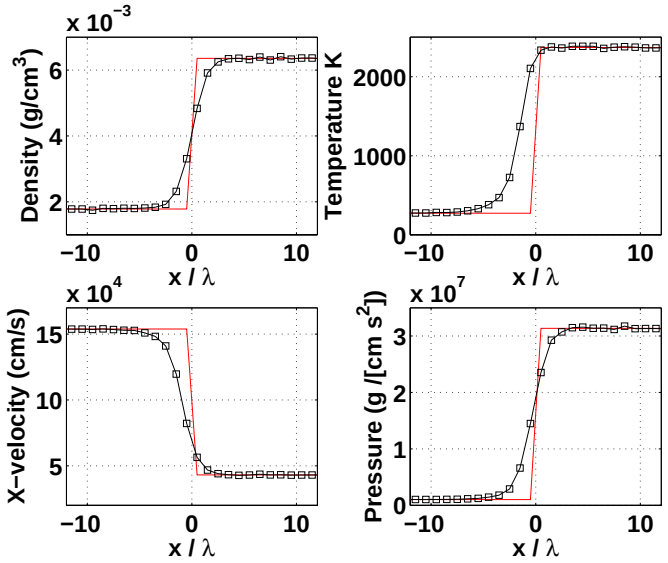

Figure 9. Equilibrium shock wave profiles for density, temperature, velocity, and pressure in the stationary Argon shock. The solid line is the theoretical result, while the solid-square line is the AMAR result.

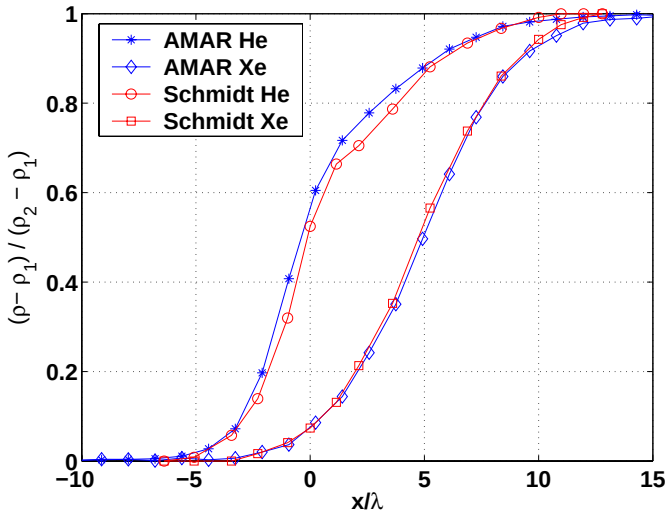

Figure 10. Comparison of He-Xe binary gas shock wave equilibrium profiles computed with AMAR (blue lines) and with DSMC alone (red lines). The mixture mean free path $\lambda = 0.46$ mm for this test.

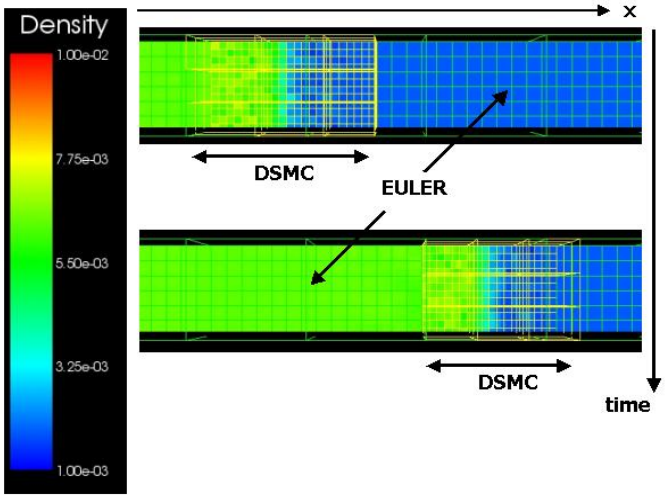

Figure 11. Moving Mach 5 shock wave though Argon. The AMAR algorithm tracks the shock by adaptively moving the DSMC region with the shock front.

$d_1 = 2.28 \times 10^{-8}$cm, $d_2 = 5.18 \times 10^{-8}$cm respectively. The upstream flow Mach number was set to 3.89 with a temperature of $300K$ and reference mass density of $1.07 \times 10^{-7} g/cm^3$. These flow conditions were chosen to allow for convenient comparison with literature results. The corresponding Rankine–Hugoniot relations for the shock density, temperature and velocity ratios are $3.34, 5.59$ and 0.3 respectively. Tolerance parameters were not used for this test and instead the refinement region was user specified to extend 15λ ahead of and 35λ behind the shock front.

Similar to the single gas shock case, the binary gas shock profile also transitions from an initial discontinuous step profile to a smoother equilibrium profile. A comparison of the equilibrium hybrid density profiles with a fully DSMC simulation performed by Schmidt and Worner [35] are shown in Figure 10. Good agreement can be seen for both Helium and Xenon density profiles.

Moving Shock Wave

Adaptive feature–tracking of the AMAR hybrid scheme is further verified using a $M = 5$ moving shock passing through a stationary Argon gas. Figure 11 shows the atomistic subdomain dynamically tracking the passage of the shock front. Similar to the case of a stationary $M = 5$ shock wave a density gradient tolerance $R_\rho = 0.2$ was found sufficient to extend the atomistic subdomain $\pm 10\lambda$ about the shock front.

The density profile of the moving shock is shown in Figure 12. Good comparison is seen with the analytical result. Note the hybrid profile does not produce spurious post–shock oscillations well–known to plague continuum–only schemes [6, 41]. Conventional shock capturing techniques for the Euler equations require artificial viscosity and enhanced smoothing techniques to reduce oscillations that cannot often be eliminated entirely. The AMAR hybrid scheme allows for accurate, adaptive and stable resolution of shock fronts without the need for artificial numerical constructs.

Our simulations also show that through a judicious choice of refinement criteria and the development of a theory to quantify the effect of fluctuations, reliable fully adaptive mesh and

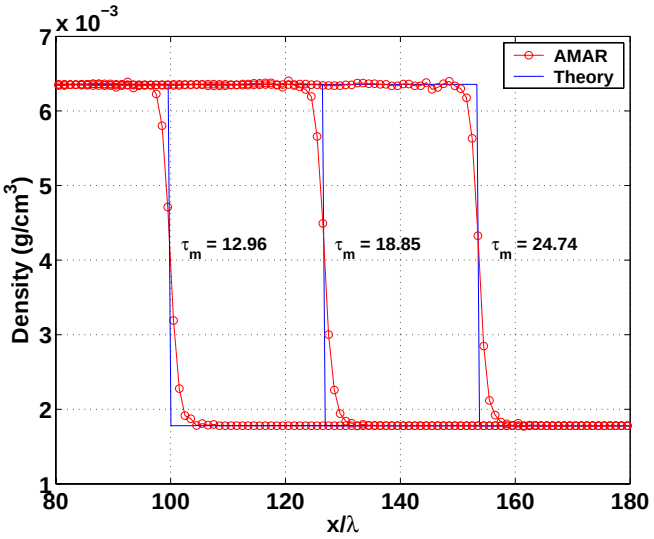

Figure 12. Moving Mach 5 shock wave though Argon. The AMAR profile (red dots) is compared with the analytical time evolution of the initial discontinuity (blue lines). τ_m is the mean collision time.

algorithm refinement algorithms are possible.

CONCLUDING REMARKS

We have described an adaptive mesh and algorithmic refinement (AMAR) scheme for modeling multi–scale, multi–species gas dynamics and have demonstrated its effectiveness in a hybrid Euler–DSMC code via a series of computational test cases. The atomistic model is applied locally in regions where the continuum description is invalid or inaccurate, such as near strong flow gradients and at fluid interfaces. In particular accurate and stable solutions for concentration diffusion, single and binary gas stationary shocks waves and moving shock waves have been obtained. These tests suggest that the AMAR code can perform highly–resolved DSMC calculations in a more cost effective manner than a DSMC–only code. An evaluation of code performance and scaling studies to larger problems will be the subject of future work.

While this effort shows the promise of the approach, much work remains to address research issues associated with such hybrid methods. In future work we plan to rigorously address issues related to accuracy and robustness of particle–continuum hybrids, criteria for adaptively switching between models, and effects of statistical fluctuations in particle schemes on the stability of continuum methods to which they may be coupled. In addition, we expect that future adoption of a Navier–Stokes model in the same algorithmic framework will yield a very useful tool for the design of micro and nano scale devices where local continuum breakdown occurs.

Finally, the range of scales and dynamic nature of multi–algorithm hybrids that may be applied to a variety of important physical problems emphasizes the need for efficient computational approaches for large–scale parallel computing platforms. The AMR grid hierarchy paradigm offers many advantages to algorithm development and parallel code implementation, including the ability to manage both field data and particles in a single grid system while allowing workload and data for each method to be distributed in parallel independently of one other. We are currently working on more effective dynamic load balancing and data distribution algorithms for our code to increase the scale of the problems we can simulate. These results will be reported in the near future.

ACKNOWLEDGMENT

The authors wish to thank B. Alder, F. Alexander, J. Bell, S. Smith, and A. Wissink for helpful discussions.

REFERENCES

[1] Abraham, F. F., Broughton, J. Q., Bernstein, N. and Kaxiras, E., *Europhysics Letters*, **44** 783 (1998).

[2] Alder, B. J., "Highly discretized dynamics", *Phys. A*, **240**, 193 (1997).

[3] Aktas, O. and Aluru, N. R., "A Combined Continuum/DSMC Technique for Multiscale Analysis of Microfluidic Filters", *Journal of Computational Physics*, **178** 342-372 (2002).

[4] Alexander, F., Garcia, A. L. and Tartakovsky D., "Algorithm Refinement for Stochastic Partial Diffential Equations: I. Linear Diffusion", *Journal of Computational Physics*, **182** No. (1), 47-66, (2002).

[5] Allen, M. P. and Tildesley, D. J., *Computer Simulation of Liquids*, (Clarendon, Oxford, 1987).

[6] Arora, M. and Roe, P. L., "On Postshock Oscillations Due to Shock Capturing Schemes in Unsteady Flows", *Journal of Computational Physics*, **130**, 25, (1997).

[7] Berger, M. and Oliger, J., "Adaptive Mesh Refinement for Hyperbolic Partial Differential Equations", *Journal of Computational Physics*, **53**, 484, (1984).

[8] Berger, M. and Colella, P., "Local Adaptive Mesh Refinement for Shock Hydrodynamics", *Journal of Computational Physics*, **82**, 64, (1989).

[9] Bird, G. A., "Breakdown of Translational and Rotational Equilibrium in Gaseous Expansions", *Am. Inst. Aero. and Astro. J.*, **8**, 1998, (1970).

[10] Bird, G. A., *Molecular Gas Dynamics and the Direct Simulation of Gas Flows*, Clarendon, Oxford, (1994).

[11] Bourgat, J., Le Tallec, P. and Tidriri, M., "Coupling Boltzmann and Navier–Stokes Equations by Friction", *Journal of Computational Physics*, **127**, 227, (1996).

[12] Colella, P., "A Direct Eulerian MUSCL Scheme for Gas Dynamics", *SIAM J. Sci. Stat. Comput.*, **6**, 104-117, (1985).

[13] Colella, P. and Glaz, H. M., "Efficient Solution Algorithms for the Riemann Problem for Real Gases", *Journal of Computational Physics*, **59**, 264-289, (1985).

[14] Flekkoy, E. G., Wagner, G. and Feder, J., "Hybrid model for combined particle and continuum dynamics", *Europhysics Letters*, **52**, 271, (2000).

[15] Garcia, A. L. and Alder, B. J., "Generation of the Chapman-Enskog Distribution", *Journal of Computational Physics*, **140**, 66, (1998).

[16] Garcia, A. L., Bell, J., Crutchfield, W. Y. and Alder, B. J., "Adaptive Mesh and Algorithm Refinement using Direct Simulation Monte Carlo", *Journal of Computational Physics*, **154**, 134, (1999).

[17] Garcia, A. L. and Wagner, W., "Time step truncation error in direct simulation Monte Carlo", *Physics of Fluids*, **12**, 2621, (2000).

[18] Hadjiconstantinou, N. G., "Analysis of Discretization in the Direct Simulation Monte Carlo", *Physics of Fluids*, **12**, 2634, 2000.

[19] Hadjiconstantinou, N. G., "Hybrid Atomistic-Continuum Formulations and the Moving Contact-Line Problem", *Journal of Computational Physics*, **154**, 245-265, (1999).

[20] Hadjiconstantinou, N. G., Simek, O., "Constant-Wall-Temperature Nusselt Number in Micro and Nano-Channels", *Journal of Heat Transfer*, **124**, 356-364, (2002).

[21] Hadjiconstantinou, N. G., "Sound wave propagation in transition-regime micro- and nanochannels", *Physics of Fluids*, **14**, 802-809, (2002).

[22] Hadjiconstantinou, N. G., "Comment on Cercignani's second-order slip coefficient", *Physics of Fluids*, **15**, 2352-2354, (2003).

[23] Hadjiconstantinou, N. G., Simek, O., "Sound propagation at small scales under continuum and non-continuum transport" *Journal of Fluid Mechanics*, **488**, 399-408, (2003).

[24] Hadjiconstantinou, N. G., Garcia, A. L., Bazant, M. Z. and He, G., "Statistical error in particle simulations of Hydrodynamic Phenomena", *Journal of Computational Physics*, **187**, pp. 274-297, (2003).

[25] Hirschfelder, J. O., Curtiss, C. F. and Bird, B., *Molecular theory of gases and liquids*, New York, Wiley (1964).

[26] Hash, D. and Hassan, H., "A Decoupled DSMC/Navier–Stokes Analysis of a Transitional Flow Experiment", *AIAA Paper* 96–0353, (1996).

[27] Hornung, R. D. and Kohn, S. R., "Managing Application Complexity in the SAMRAI Object-Oriented Framework", *Concurrency and Computation: Practice and Experience*, **14**, 347-368 (2002).

[28] Le Tallec, P. and Mallinger, F., "Coupling Boltzmann and Navier–Stokes Equations by Half Fluxes", *Journal of Computational Physics*, **136**, 51, (1997).

[29] Li, J., Liao, D. and Yip, S., "Coupling continuum to molecular-dynamics simulation: Reflecting particle method and the field estimator", *Physical Review E*, **57**, 7259–7267 (1998).

[30] O'Connell, S. T., and Thompson, P. A., "Molecular dynamics-continuum hybrid computations: A tool for studying complex fluid flows", *Physical Review E*, **52** R5792–R5795 (1995).

[31] Roveda, R., Goldstein, D. B. and Varghese, P. L., "Hybrid Euler/direct simulation Monte Carlo calculation of unsteady slit flow", *Journal of Spacecraft and Rockets*, **37** No. 6, pp. 753–760, (2000).

[32] Rudd, R. E., Broughton, J. Q., "Concurrent coupling of length scales in solid state systems", *Phys. Status Solidi B*, **217**, 251, (2000).

[33] Saltzman, J., "An Unsplit 3D Upwind Method for Hyperbolic Conservation Laws", *Journal of Computational Physics*, **115**, 153, (1994).

[34] Vahedi, V. and Surendra, M., "Monte-Carlo collision model for particle-in-cell method: application to argon and oxygen discharges", *Comput. Phys. Commun.*, **87**, 179-98, (1995).

[35] Schmidt, B. and Worner, M., "Problems with the Computation of the Shock Structure in Binary Gas Mixtures Using the Direct Simulation Monte Carlo Method", *Acta Mechanica* (1-4), pp. 59–55, (1983).

[36] Shenoy, V. B., Miller, R., Tadmor, E. B., Rodney, D., Phillips, R. and Ortiz M., "An Adaptive Finite Element Approach to Atomic-Scale Mechanics – The Quasicontinuum Method", *J. Mechanics and Phys. Solids*, **47**, 611, (1999).

[37] Tiwari, S. and Klar, A., "Coupling of the Boltzmann and Euler equations with adaptive domain decomposition procedure", *Journal of Computational Physics*, **144**, 710, (1998).

[38] Trangenstein, J.A. and R.B. Pember, "Numerical Algorithms for Strong Discontinuities in Elastic-Plastic Solids", *Journal of Computational Physics*, **103**, 63–89, (1992).

[39] Wadsworth, D. C. and Erwin, D. A., "One-Dimensional Hybrid Continuum/Particle Simulation Approach for Rarefied Hypersonic Flows", *AIAA Paper*, 90–1690, (1990).

[40] Wagner, W., "A Convergence Proof for Bird's Direct Simulation Monte Carlo Method for the Boltzmann Equation", *Journal of Statistical Physics*, **66**, 1011, (1992).

[41] Woodward, P. R. and Colella, P., "The Numerical Simulation of Two-dimensional Fluid Flow with Strong Shocks", *Journal of Computational Physics*, **54**, 115, (1984).